EXTENDED NONLINEAR ANALYTICAL MODELS OF COMPLIANT PARALLELOGRAM MECHANISMS: THIRD-ORDER MODELS

Guangbo Hao
School of Engineering, University College Cork, Cork, Ireland
E-mail: G.Hao@ucc.ie

Received Month January 2014, Accepted Month May 2014
No. 14-CSME-01, E.I.C. Accession Number 3663

ABSTRACT

This paper proposes extended nonlinear analytical models, third-order models, of compliant parallelogram mechanisms. These models are capable of capturing the accurate effects from the very large axial force within the transverse motion range of 10% of the beam length through incorporating the terms associated with the high-order (up to third-order) axial force. A case study of the compound compliant parallelogram mechanism, composed of two basic compliant parallelogram mechanisms in symmetry, is also implemented. It is shown that in the case study the slenderness ratio affects the result discrepancy between the third-order model and the first-order model significantly, and the third-order model can illustrate a non-monotonic transverse stiffness curve if the beam is thin enough.

Keywords: compliant mechanism; parallelogram; nonlinearity; third-order model; guided beam.

MODÈLES ANALYTIQUES NON LINÉAIRES ÉTENDUES DES MÉCANISMES À PARALLÉLOGRAMME CONFORMES: MODÈLES DU TROISIÈME ORDRE

RÉSUMÉ

Cet article propose des modèles non linéaires étendues analytiques, des modèles du troisième ordre, des mécanismes à parallélogramme conformes. Ces modèles sont capables de capturer les effets précis de la force axiale très grande au sein de la gamme de mouvement transversal de 10% de la longueur de la poutre en intégrant les termes associés à l'ordre élevé (jusqu'à troisième ordre) de la force axiale. Une étude de cas du mécanisme à parallélogramme composé, composé de deux mécanismes en parallélogramme de base conformes à la symétrie, est en outre mis en oeuvre. Il est démontré que dans l'étude de cas, le rapport d'élancement affecte la différence de résultat entre le modèle du troisième ordre et le modèle du premier ordre de manière significative, et le modèle du troisième ordre peut illustrer une courbe de raideur transversale non - monotone si le faisceau est assez mince.

Mots-clés : mécanisme conforme; parallélogramme; non-linéarité; modèle du troisième ordre; faisceau guidée.

1 INTRODUCTION

Compliant parallelogram mechanisms have been being extensively used in the fields of precision engineering and MEMS (microelectromechanical systems) as compliant translational joints or force sensors [1]. A popularly used compound compliant parallelogram mechanism, composed of two basic parallelogram mechanisms in symmetry, is shown in Fig. 1 as an example [2]. It is always desired to derive simple enough but quite accurate mathematical models for the compliant parallelogram mechanisms to provide quick design and analysis in comparison with the FEA (finite element analysis) and experimental methods.

Traditional linear analytical analysis [3] has limited applications for compliant mechanisms usually only providing an initial estimate for deformed displacements as a reference for nonlinear analysis. To capture the nonlinearities of force-displacement equations[1], the load-equilibrium conditions for a cantilever beam should be applied in the deformed configuration of compliant mechanisms [4], which is different from the configuration before deformation as used in linear load-equilibrium conditions. Awtar [4,5] derived nonlinear and analytical force-displacement equations of a basic cantilever beam, which are able to offer a very accurate estimation for the mobile end displacements under given loading if the transverse motion range of the mobile end is less than 10% of the beam length (to ensure that the rotational angle of any point along the beam is lower than 0.1 radians). It can be concluded from Awtar's work that the axial force is the dominant factor contributing to the nonlinearity. Zelenika et al [6] also proposed nonlinear equations of the compliant beam in a cross-spring pivot in the deformed configuration using a numerical method. In addition, other nonlinear methods such as a comprehensive elliptic integral solution (incorporating post-duckling behavior) [7] or 3R (R: revolute joint) PRBMs (pseudo-rigid-body models) [8,9] were employed to obtain the accurate load-displacements relations. Nevertheless, these models presented in [6–9] are hard to use for modeling the system composed of multiple beams due to the limitation and/or the complication of solutions.

Using the nonlinear analytical model of the single beam, Ref. [5] reported a simple nonlinear analytical model for a compliant parallelogram mechanism and analyzed its nonlinear characteristics. But this model only involves the contribution from the terms associated with the first-order axial force but ignores the terms associated with the higher-order axial force, which brings an error less than 5% if the normalized axial force magnitude is less than 10. This work reveals the fact that any difference in the axial forces acting on the beams will cause an unequal transverse stiffness change in the beams, and result in a rotational yaw. However, this model in [5] for the compliant parallelogram mechanism, without considering the terms associated the high-order axial force, is not suitable for certain case that the axial force is very large as the example in Fig. 1 in the large-range motion. In addition, PRBMs in [2,10] were adopted to deal with the compliant parallelogram mechanism, but still have difficulty and complexity in considering the pure elasticity and the center drift of pseudo-rotational joint, and therefore cannot accurately capture the parasitic translation and the parasitic rotation effects.

Based on the above advances, this paper aims to extend the nonlinear analytical models of compliant parallelogram mechanisms to capture the accurate effects from the very large axial force by including the terms associated with the high-order axial force (up to third order). This paper is organized as follows.

[1]Non-linearity in force-displacement characteristics of a basic cantilever beam (Euler–Bernoulli beam) has three sources: material non-linearity, geometric non-linearity and non-linearity of load-equilibrium equations. The material non-linearity can be neglected for most applications and the geometric non-linearity will also be ignored in this paper because the transverse displacement range is limited to be less than 0.1 of the beam length. The non-linearity of load-equilibrium equations should be always considered for a cantilever beam even though the deformation is very small, which applies the load-equilibrium conditions in the deformed configuration of compliant mechanisms.

An extended model of the basic compliant parallelogram mechanism for the nonlinear analytical analysis is shown in Section 2. Section 3 further derives nonlinear analytical models of compliant multi-beam parallelogram mechanisms with guided motion stage. A case study is then conducted in Section 4 to discuss the load-displacement relations and the primary stiffness characteristic of the compound compliant parallelogram mechanism. Conclusions are drawn finally.

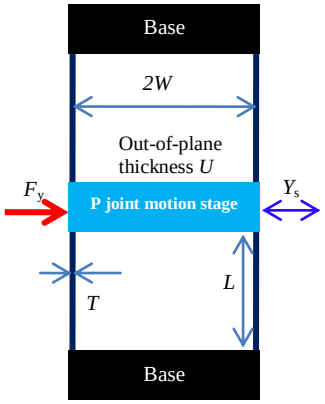

Fig. 1. A compound compliant parallelogram mechanism.

2 NONLINEAR ANALYTICAL MODEL FOR A BASIC COMPLIANT PARALLELOGRAM MECHANISM

There are two main methods of solving force-displacement relations for compliant mechanisms: a) the free-body diagram method [4]; and b) the energy based method such as virtual work principle [11]. Compared with the free-body diagram method, the energy based method can reduce the number of unknown variables via eliminating the internal load variables. However, the internal loads are desirable in compliant mechanisms for estimating stress level. Also, due to the involved non-linearity, it will be extremely complex to invert these relations to obtain displacements in terms of forces as demonstrated in [11], which are ultimately desired in the analysis. Therefore, the free-body diagram method will be used in this section to derive the nonlinear analytical model for the basic compliant parallelogram mechanism.

Note that normalization strategy is employed throughout the derivations in Sections 2 and 3, which refers to that all translational displacements and length parameters are normalized by the beam actual length L, forces by EI/L^2, and moments by EI/L. Here, E denotes the Young's modulus, and I represents the second moment of the area of a rectangular cross section. The corresponding lower-case letters are used to denote the normalized ones.

A compliant parallelogram mechanism in the deformed configuration is shown in Fig. 2. The external loads, exerted on the motion stage center of the parallelogram mechanism, are denoted as p (axial force along the X-axis), f (transverse force along the Y-axis), and m (moment about the Z-axis), and displacements of the motion stage center are represented by x_s (axial displacement along the X-axis), y_s (transverse displacement along the Y-axis), and θ_s (rotation about the Z-axis). Other internal loads (p_1, f_1, and m_1 or p_2, f_2, and m_2) and displacements (x_1, y_1, and θ_1 or x_2, y_2, and θ_2) for the mobile end of each single beam are detailed in Fig. 2. The purpose of this section is to derive the more accurate load-displacement relations, third-order models, of the compliant parallelogram mechanism on the basis of the load-displacement equations of a single beam, geometry compatibility conditions and load-equilibrium conditions.

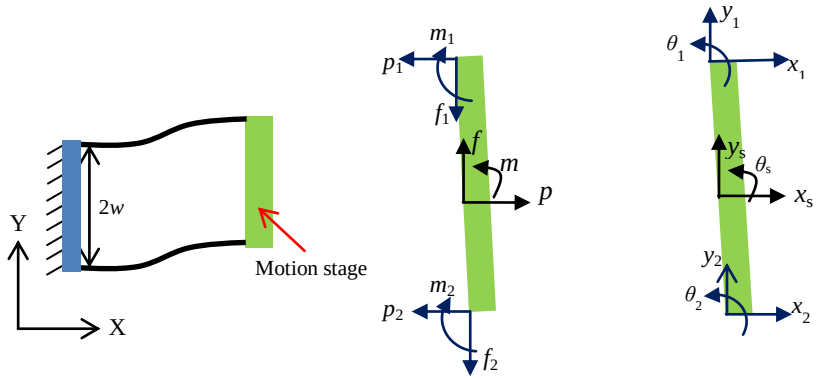

Fig. 2. Compliant parallelogram mechanism in deformation.

1) *Load-displacement relations of a single beam*

Using the research results in [5] by retaining the terms associated with the high-order axial force of the load-displacement equations of a single beam, one can obtain

$$\begin{aligned}\begin{bmatrix} f_i \\ m_i \end{bmatrix} &= \begin{bmatrix} 12 & -6 \\ -6 & 4 \end{bmatrix}\begin{bmatrix} y_i \\ \theta_i \end{bmatrix} + p_i \begin{bmatrix} 6/5 & -1/10 \\ -1/10 & 2/15 \end{bmatrix}\begin{bmatrix} y_i \\ \theta_i \end{bmatrix} \\ &+ p_i^2 \begin{bmatrix} -1/700 & 1/1400 \\ 1/1400 & -11/6300 \end{bmatrix}\begin{bmatrix} y_i \\ \theta_i \end{bmatrix} + p_i^3 \begin{bmatrix} 1/63000 & -1/1260000 \\ -1/1260000 & 1/27000 \end{bmatrix}\begin{bmatrix} y_i \\ \theta_i \end{bmatrix},\end{aligned} \tag{1}$$

$$\begin{aligned}x_i &= \frac{1}{d} p_i + [y_i, \theta_i]\begin{bmatrix} -3/5 & 1/20 \\ 1/20 & -1/15 \end{bmatrix}\begin{bmatrix} y_i \\ \theta_i \end{bmatrix} + p_i [y_i, \theta_i]\begin{bmatrix} 1/700 & -1/1400 \\ -1/1400 & 11/6300 \end{bmatrix}\begin{bmatrix} y_i \\ \theta_i \end{bmatrix} \\ &+ p_i^2 [y_i, \theta_i]\begin{bmatrix} -1/42000 & 1/84000 \\ 1/84000 & -1/18000 \end{bmatrix}\begin{bmatrix} y_i \\ \theta_i \end{bmatrix} + p_i^3 [y_i, \theta_i]\begin{bmatrix} 37/97020000 & -37/194040000 \\ -37/194040000 & 509/291060000 \end{bmatrix}\begin{bmatrix} y_i \\ \theta_i \end{bmatrix}\end{aligned} \tag{2}$$

where i=1 or 2. d is equal to $12/(T/L)^2$, which is a dimensionless parameter related to the slenderness ratio. Here, T is the in-plane thickness of the beam, and L is the length of the beam.

2) *Geometry compatibility conditions*

Based on the free body diagram in Fig. 2, one can have the geometry compatibility conditions as

$$x_1 = x_s - w\theta_s, \tag{3}$$

$$x_2 = x_s + w\theta_s, \tag{4}$$

$$y_1 = y_2 = y_s, \tag{5}$$

$$\theta_1 = \theta_2 = \theta_s. \tag{6}$$

3) *Load-equilibrium conditions*

Load-equilibrium conditions can further derived from Fig. 2 as follows:

$$p = p_1 + p_2, \tag{7}$$

$$f = f_1 + f_2, \tag{8}$$

$$m = m_1 + m_2 + (p_2 - p_1)w + (f_2 - f_1)w\theta_s \approx m_1 + m_2 + (p_2 - p_1)w. \tag{9}$$

4) *Nonlinear analytical modeling*

From Eqs. (2), (3), (4), (5) and (7), one can derive

$$x_s = \frac{(x_1 + x_2)}{2}$$
$$\approx \frac{1}{2d} p + (-3/5) y_s^2 + \frac{(1/700) y_s^2 p}{2} + \frac{(-1/42000) y_s^2 (p_1^2 + p_2^2)}{2} + \frac{(37/97020000) y_s^2 (p_1^3 + p_2^3)}{2} \quad . \tag{10}$$

The parasitic rotational angle, θ_s, can be derived on the basis of Eqs. (3), (4), (5) and (7) as

$$\theta_s = \frac{(x_2 - x_1)}{2w}$$
$$\approx \frac{1}{2w}[\frac{1}{d}(p_2 - p_1) + (1/700) y_s^2 (p_2 - p_1) + (-1/42000) y_s^2 (p_2^2 - p_1^2) + (37/97020000) y_s^2 (p_2^3 - p_1^3)] \quad . \tag{11}$$

The terms associated with the high-order internal axial force in Eqs. (10) and (11) can be represented as follows:

$$(p_1^2 + p_2^2) = \frac{(p_1 + p_2)^2 + (p_2 - p_1)^2}{2} = \frac{p^2 + (p_2 - p_1)^2}{2}, \tag{12}$$

$$(p_1^3 + p_2^3) = (p_1 + p_2)^3 - 3pp_1p_2 = p^3 - 3pp_1p_2, \tag{13}$$

$$(p_2^2 - p_1^2) = p(p_2 - p_1), \tag{14}$$

$$(p_2^3 - p_1^3) = (p_2 - p_1)(p_1^2 + p_2^2 + p_1p_2), \tag{15}$$

where

$$p_1 p_2 = \frac{(p_1 + p_2)^2 - (p_2 - p_1)^2}{4} = \frac{p^2 - (p_2 - p_1)^2}{4} \quad . \tag{16}$$

Therefore, all the above high-order terms in Eqs. (12)–(15) can be represented as the function of (p_2–p_1).

From Eq. (9), the following is obtained

$$(p_2 - p_1) = \frac{m - (m_1 + m_2)}{w} \quad . \tag{17}$$

The substitution of Eq. (17) into Eqs. (12)–(16) yields

$$(p_1^2 + p_2^2) = \frac{p^2 + (\frac{m - (m_1 + m_2)}{w})^2}{2} = \frac{p^2 w^2 + [m - (m_1 + m_2)]^2}{2w^2}, \tag{18}$$

$$(p_1^3 + p_2^3) = p^3 - 3p\frac{p^2 - [\frac{m - (m_1 + m_2)}{w}]^2}{4} = p^3 - 3p\frac{p^2 w^2 - [m - (m_1 + m_2)]^2}{4w^2}, \tag{19}$$

$$(p_2^2 - p_1^2) = p\frac{m - (m_1 + m_2)}{w}, \tag{20}$$

$$(p_2^3 - p_1^3) = \frac{m - (m_1 + m_2)}{w}\{\frac{p^2 w^2 + [m - (m_1 + m_2)]^2}{2w^2} + \frac{p^2 w^2 - [m - (m_1 + m_2)]^2}{4w^2}\}$$
$$= \frac{m - (m_1 + m_2)}{w}\{\frac{3p^2 w^2 + [m - (m_1 + m_2)]^2}{4w^2}\} \quad . \tag{21}$$

The next step is to derive the expression of (m_1+m_2) from Eq. (1) as

$$m_1+m_2=(-6y_s+4\theta_s)+p_1(-\frac{1}{10}y_s+\frac{2}{15}\theta_s)+p_1^2(\frac{1}{1400}y_s-\frac{11}{6300}\theta_s)+p_1^3(-\frac{1}{1260000}y_s+\frac{1}{2700}\theta_s)$$
$$+(-6y_s+4\theta_s)+p_2(-\frac{1}{10}y_s+\frac{2}{15}\theta_s)+p_2^2(\frac{1}{1400}y_s-\frac{11}{6300}\theta_s)+p_2^3(-\frac{1}{1260000}y_s+\frac{1}{2700}\theta_s)$$
$$=[-12-\frac{1}{10}p+\frac{1}{1400}(p_1^2+p_2^2)-\frac{1}{1260000}(p_1^3+p_2^3)]y_s+[8+\frac{2}{15}p-\frac{11}{6300}(p_1^2+p_2^2)+\frac{1}{2700}(p_1^3+p_2^3)]\theta_s$$
$$\approx[-12-\frac{1}{10}p+\frac{1}{1400}(p_1^2+p_2^2)-\frac{1}{1260000}(p_1^3+p_2^3)]y_s \quad (22)$$

Similar to Eq. (22), the combination of Eqs. (1) and (8) results in

$$f=f_1+f_2$$
$$=[24+\frac{6}{5}p-\frac{1}{700}(p_1^2+p_2^2)+\frac{1}{63000}(p_1^3+p_2^3)]y_s+[-12-\frac{1}{10}p+\frac{1}{1400}(p_1^2+p_2^2)-\frac{1}{1260000}(p_1^3+p_2^3)]\theta_s$$
$$\approx[24+\frac{6}{5}p-\frac{1}{700}(p_1^2+p_2^2)+\frac{1}{63000}(p_1^3+p_2^3)]y_s \quad (23a)$$

Equation (23a) can be further re-written as

$$y_s=\frac{f}{[24+\frac{6}{5}p-\frac{1}{700}(p_1^2+p_2^2)+\frac{1}{63000}(p_1^3+p_2^3)]}. \quad (23b)$$

The result of the substitution of Eq. (23b) into Eq. (22) is the function of two variables, $A=(p_1^2+p_2^2)$ and $B=(p_1^3+p_2^3)$, which can be further substituted back into Eqs. (18) and (19) to obtain the solutions for $(p_1^2+p_2^2)$ and $(p_1^3+p_2^3)$ if the loading is known. If p=0, then $(p_1^3+p_2^3)$=0 and $p_1^2=p_2^2=A/2$ on the basis of Eq. (13). Once $(p_1^2+p_2^2)$ and $(p_1^3+p_2^3)$ are obtained, the following procedure can be used to obtain the displacements under known loading (i.e. forward solutions):

a) y_s is obtained first based on the use of Eq. (23b).

b) (m_1+m_2) and x_s can be then obtained through substituting y_s into Eqs. (22) and (10).

c) Equations (17), (20) and (21) are further solved.

d) The rotational angle θ_s is finally obtained via substituting all known conditions into Eq. (11).

Based on the above procedure, one can obtain all the solutions for the displacements, y_s, x_s and θ_s, under the action of loading without applied moment as shown in Fig. 3 as an example demonstration. It can be observed from Fig. 3(a–c) that the smaller p is, the more significant the displacement change affect by the transverse force is.

In addition, if all the displacements are specified, the following procedure can be adopted to obtain the required loads (i.e. inverse solutions):

a) Equations (10) and (11) are firstly used to get the solutions for p and (p_2–p_1) since x_s and θ_s are both the functions of them by observing Eqs. (12)–(16).

b) $(p_1^2+p_2^2)$ and $(p_1^3+p_2^3)$ are then obtained from Eqs. (12) and (13) with the help of Eq. (16).

c) The transverse force f is further solved using Eq. (23a).

d) The moment m is finally obtained from Eq. (9) in combination with Eq. (22).

Note that the major advantage of the proposed third-order model is the much more accurate inverse solutions than the first-order model proposed in [5] once the displacements are known, which will be shown in the Section 4. However, there are still certain limitations for the above proposed third-order analytical model similar to the first-order model. For example, the post-buckling behavior is not incorporated and large-deformation characteristics (normalized transverse motion range much larger than 0.1) cannot be accurately captured in the third-order model proposed in this paper.

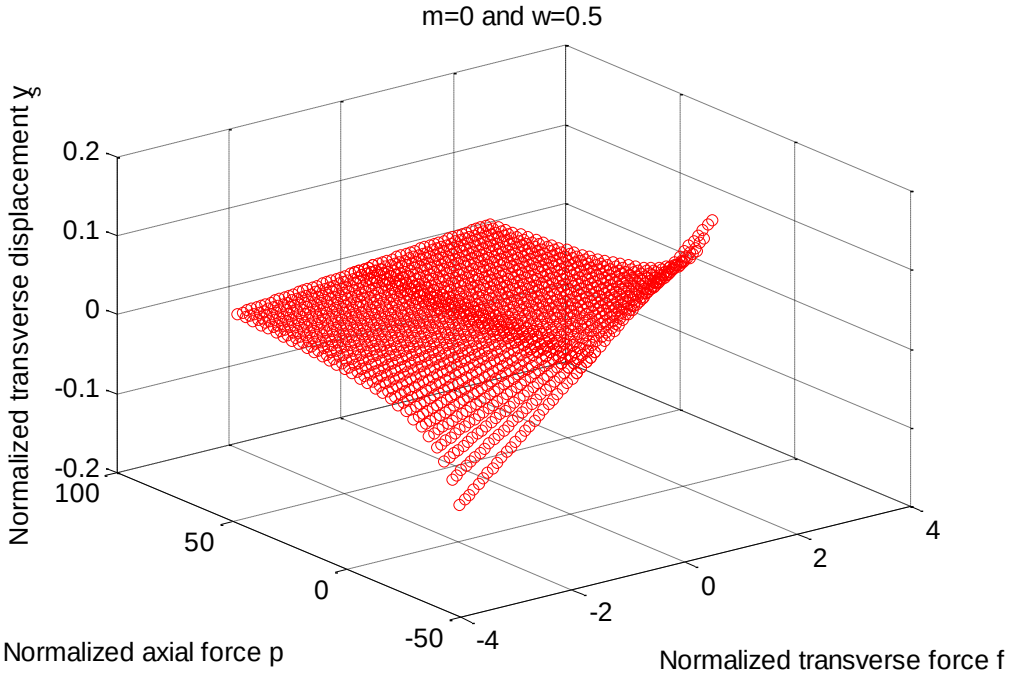

(a)

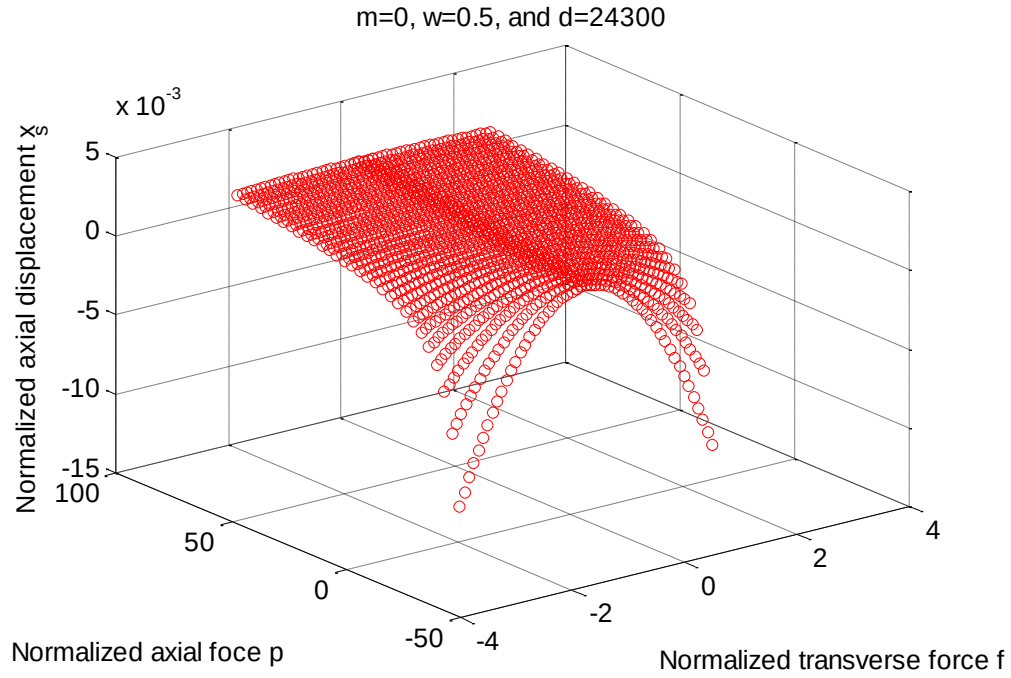

(b)

Fig. 3. Solutions for the displacements under given loading (continued on next page)

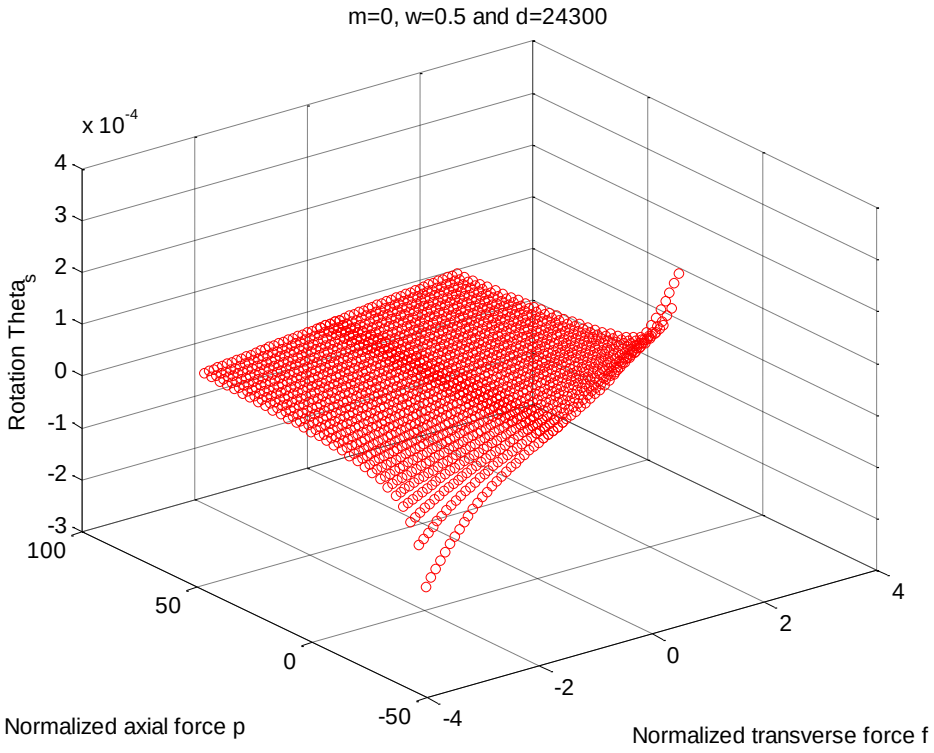

(c)

Fig. 3. Solutions for the displacements under given loading: (a) transverse displacement; (b) axial displacement; (c) rotational angle.

3 NONLINEAR ANALYTICAL MODELS FOR GUIDED COMPLIANT MULTI-BEAM PARALLELOGRAM MECHANISMS

This section only deals with the guided compliant parallelogram mechanism with multiple beams (beam number is n), which means that the parasitic rotation of the motion stage is constrained to zero.

1) *Case 1*

If n=2, the case is the basic parallelogram mechanism as discussed in Section 2. In the case of θ_s=0, it can be obtained that p_1=p_2=p/2 from Eqs. (11) and (7). Therefore, the translational displacement equations are derived from Eqs. (23b) and (10) as follows:

$$y_s = \frac{f}{24 + \frac{6}{5}p - \frac{1}{700}\frac{p^2}{2} + \frac{1}{63000}\frac{p^3}{4}}, \tag{24}$$

$$x_s = \frac{1}{2d}p + y_s^2\left[-(3/5) + \frac{(1/700)p}{2} - \frac{(1/42000)}{2}\frac{p^2}{2} + \frac{(37/97020000)}{2}\frac{p^3}{4}\right]. \tag{25}$$

2) *Case 2*

If n=2N (N is integral), the case is the compliant multi-beam parallelogram mechanism as shown in Fig. 4. For convenient studying, the beams are divided into N groups so that each group is a basic compliant parallelogram mechanism with two beams equally displaced with regard to the motion stage center (Fig. 4).

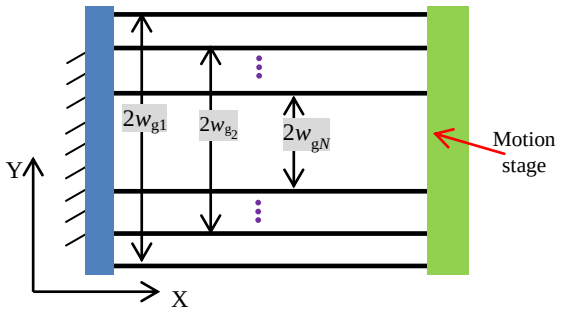

Fig. 4. Compliant multi-beam parallelogram mechanism.

The nonlinear analytical modeling of the guided compliant multi-beam parallelogram mechanism can be derived from the solutions of the basic parallelogram mechanism (Fig. 2). The motion stage center is specified as the position of the output displacements or the applied external loads of the multi-beam parallelogram mechanism with the same definition as the above. This center is also the specified point of the displacements and loads for the individual basic parallelogram mechanism.

The external loads, p, f and m, are also split into N groups denoted by p_{g1}, f_{g1} and m_{g1} (group 1); p_{g2}, f_{g2} and m_{g2} (group 2); …; p_{gi}, f_{gi} and m_{gi} (group i; here, i=1, 2, 3 until N); …; p_{gN}, f_{gN} and m_{gN} (group N) exerted on N basic compliant parallelogram mechanisms. Then the following load-equilibrium equations can be obtained as

$$\begin{cases} p_{g1} + p_{g2} + p_{g3} + ,...,+ p_{gN} = p \\ f_{g1} + f_{g2} + f_{g3} + ,...,+ f_{gN} = f \\ m_{g1} + m_{g2} + m_{g3} + ,...,+ m_{gN} = m \end{cases} . \tag{26}$$

Using the results in Eqs. (24) and (25), one can obtain

$$\begin{cases} y_s = y_{gi} = \dfrac{f_{gi}}{24 + \dfrac{6}{5} p_{gi} - \dfrac{1}{700} \dfrac{p_{gi}^2}{2} + \dfrac{1}{63000} \dfrac{p_{gi}^3}{4}} \\ x_s = x_{gi} = \dfrac{1}{2d} p_{gi} + y_s^2 [-(3/5) + \dfrac{(1/700) p_{gi}}{2} - \dfrac{(1/42000)}{2} \dfrac{p_{gi}^2}{2} + \dfrac{(37/97020000)}{2} \dfrac{p_{gi}^3}{4}] \end{cases} \tag{27}$$

where y_{gi} and x_{gi} are the translational displacements of the i-th individual basic parallelogram mechanism.

The combination of Eqs. (26) and (27) then gives that

$$\begin{cases} p_{g1} = p_{g2} = p_{g3} = ,...,= p_{gN} = p / N \\ f_{g1} = f_{g2} = f_{g3} = ,...,= f_{gN} = f / N \end{cases} . \tag{28}$$

Therefore, using the results in Eq. (28), Eq. (27) is re-written as

$$\begin{cases} y_s = \dfrac{f}{N(24 + \dfrac{6}{5} \dfrac{p}{N} - \dfrac{1}{700} \dfrac{p^2}{2N^2} + \dfrac{1}{63000} \dfrac{p^3}{4N^3})} \\ x_s = \dfrac{1}{2d} \dfrac{p}{N} + y_s^2 [-(3/5) + \dfrac{(1/700)}{2} \dfrac{p}{N} - \dfrac{(1/42000)}{2} \dfrac{p^2}{2N^2} + \dfrac{(37/97020000)}{2} \dfrac{p^3}{4N^3}] \end{cases} . \tag{29}$$

The buckling for a multi-beam parallelogram mechanism occurs if the denominator of the transverse displacement equation in Eq. (29) becomes zero. In the case of N=1, the normalized buckling load is p_c=19.74. From the classic mechanics for the guided basic parallelogram mechanism [12], it is learnt that

the actual buckling load is $p_c=2\pi^2=19.74$, which is exactly same as the result predicted by the third-order model in Eq. (29). However, if the terms associated with the high-order axial force are neglected, i.e. the first-order model [5] is used, the buckling load can be solved to be $p_c=20$, which is a little larger than the actual result.

4 CASE STUDY

In this section, the compound compliant parallelogram mechanism (Fig. 1) will be analyzed if only the force along the primary motion direction is applied. The non-normalized geometrical parameters for a typical example are shown as follows: W=10 mm, L=45 mm, T=1 mm and U=20 mm. The material Young's modulus, E, is set up to be 69 GPa with the Poisson ratio, v, of 0.33. Nonlinear finite element analysis (FEA) is used in this section to simulate the load-displacement relations of this example.

In the case that only one force, f_y, is applied on the motion stage (Fig. 1), each basic parallelogram mechanism is end-guided due to the symmetry, and the transverse force along the Y-axis on each is $f_y/2$. The following conditions for each individual basic parallelogram mechanism should be satisfied based on Eqs. (24) and (25):

$$y_s = \frac{f_y/2}{24+\frac{6}{5}p-\frac{1}{700}\frac{p}{2}^2+\frac{1}{63000}\frac{p}{4}^3}, \tag{30}$$

$$x_s = \frac{1}{2d}p + y_s^2[-(3/5)+\frac{(1/700)p}{2}-\frac{(1/42000)}{2}\frac{p^2}{2}+\frac{(37/97020000)}{2}\frac{p^3}{4}] = 0 \tag{31}$$

where p is internal axial force (positive) on the individual basic parallelogram mechanism. So the internal axial force on each beam is $p/2$.

In order to obtain the solutions to Eqs. (30) and (31), the internal axial force, p, is firstly solved from Eq. (31) once the transverse displacement y_s is specified. Then, the internal force, p, is substituted into Eq. (30) to obtain the external force, f_y, so that the load-displacement relation curve for the compound compliant parallelogram mechanism can be plotted finally. Furthermore, the transverse stiffness change with the transverse motion can be calculated by df_y/dy_s using the above obtained load-displacement relation. It should be noted that when solving for the internal axial force, three solutions, one real and two imaginary, can be obtained due to the third-order model. However, only the real solution is the desired one.

Three models, FEA model, third-order model and first-order model, are employed to show the non-normalized load-displacement relations in Fig. 5 for the specified example. It is revealed that the third-order model has a very good agreement with the nonlinear FEA model in the whole transverse motion range (less than 10% of the beam length) but the first-order model [5] well coincides with the third-order model or the FEA model before 3mm.

The normalized internal axial force change, the normalized transverse force change, and the normalized transverse stiffness change with the transverse motion and the parameter d are elaborated in Figs. 6, 7, and 8. It is suggested that the parameter d affects the discrepancy between the third-order model and the first-order model significantly. The larger d is (the thinner the beam), the larger the discrepancy is (the smaller the coincidence domain between the two models). This means that if the beam is thick enough, the first-order model can be used to well predict the load-displacement behavior even under the very large axial force.

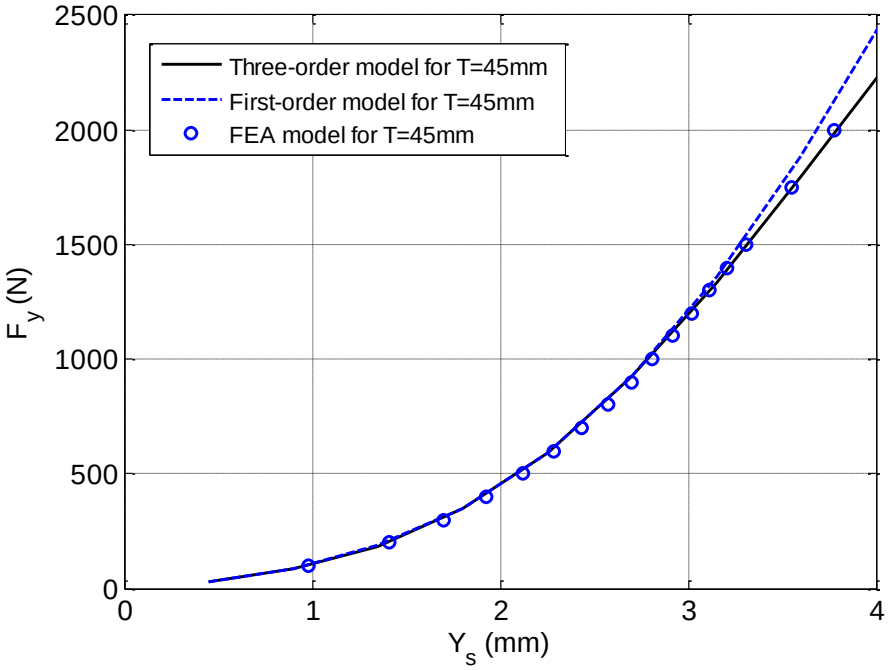

Fig. 5. Comparison of three models for the typical example.

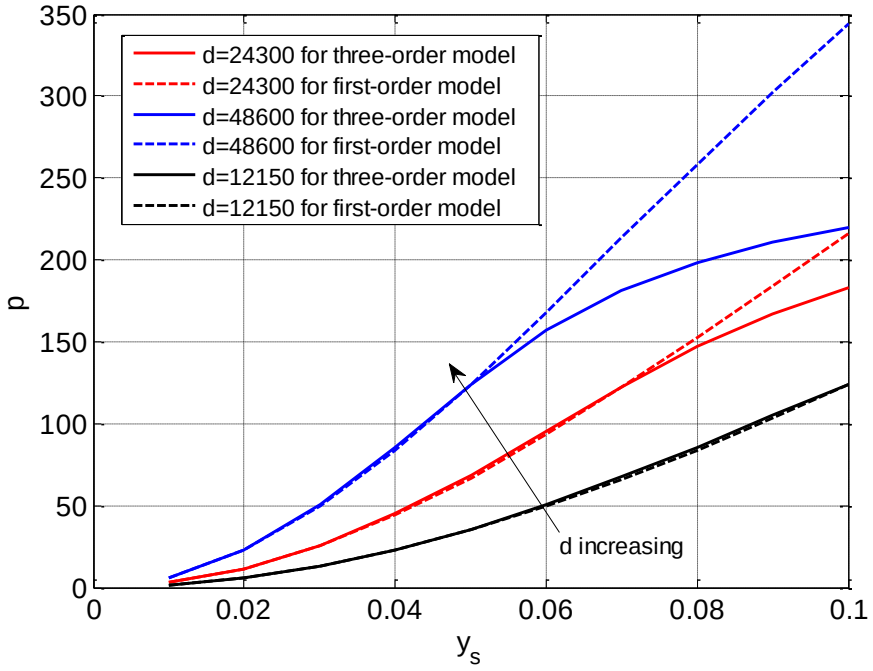

Fig. 6. Internal axial force change with the transverse motion.

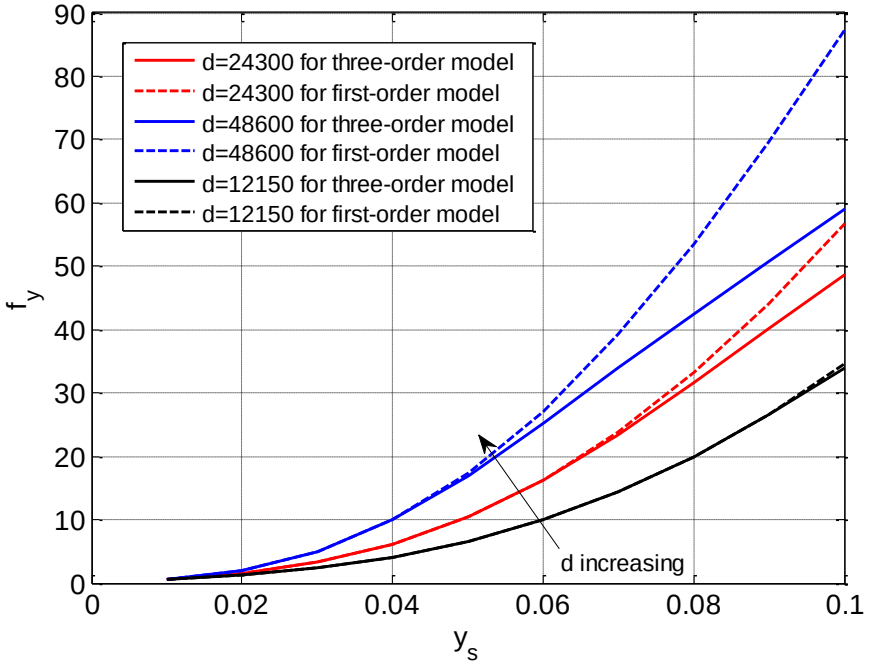

Fig. 7. Transverse force change with the transverse motion.

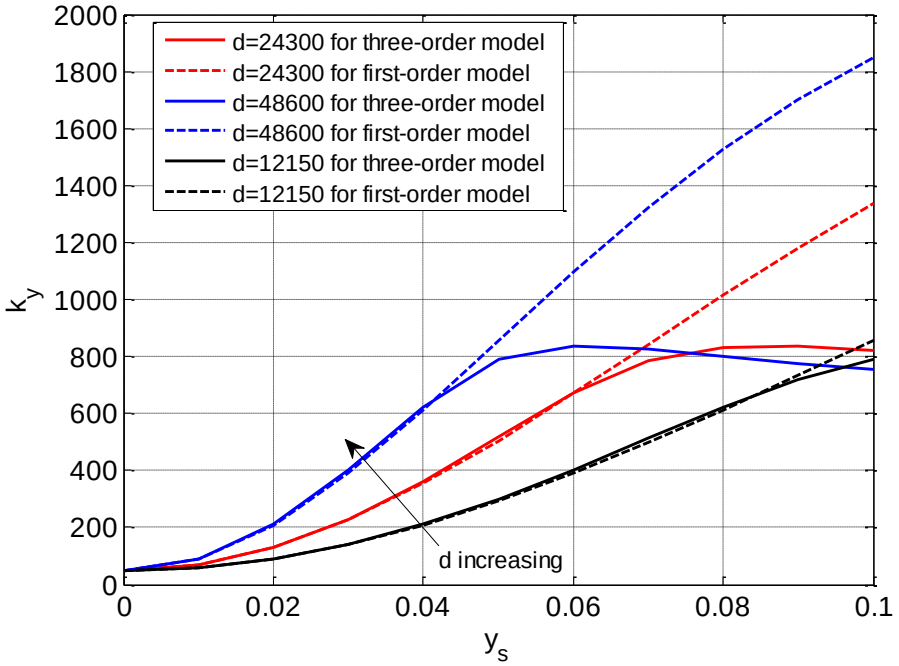

Fig. 8. Transverse stiffness change with the transverse motion.

In addition, Figs. 6 and 7 show that the increase of *d* also brings the increase of the force (internal axial force or the transverse force) under the same transverse motion for both the first-order and third-order models. In Fig. 8, the first-order model estimates a different transverse stiffness trend from the one estimated by the third-order model. The first-order model always shows a monotonic stiffness curve,

while the third-order model can illustrate a non-monotonic stiffness curve if d is large enough. Note that for d=24300, the transverse stiffness at y_s=0.1 is about 18 times larger than that at y_s=0, which implies that transverse direction (primary motion) of the compound compliant parallelogram mechanism degrades from a DOF (degree of freedom) to a DOC (degree of constraint).

5 CONCLUSIONS

Extended nonlinear analytical models have been developed in this paper for the basic parallelogram mechanism and the guided multi-beam parallelogram mechanisms. The proposed models are third-order models, which can reflect the accurate effects from the very large axial force within the transverse motion range (10% of the beam length) through incorporating the terms associated with the high-order (up to third-order) axial force. The proposed third-order model provides the much more accurate inverse solutions than the first-order model once the displacements are known. The buckling load for the guided compliant multi-beam parallelogram mechanism can also be accurately calculated using the three-order model.

The load-displacement relations and the transverse stiffness characteristic over the whole transverse motion range for the compound parallelogram mechanism have been analyzed in details based on the third-order model of the guided basic parallelogram mechanism. The FEA and first-order models have been compared with the third-order model. FEA results have validated the third-order model and confirmed the slight inaccuracy of the first-order model in the case study. It has been shown that the slenderness ratio of the beam influences the deviation of the first-order model from the third-order model significantly, and the first-order model is only valid if the motion range is relatively small or the beam is thick enough. In addition, the third-order model can illustrate a non-monotonic transverse stiffness curve if the beam is thin enough.

It is noted that the present third-order model cannot capture the post-buckling behavior, but can still provide quick design and analysis for the compliant parallelogram mechanisms in most engineering applications.

6 REFERENCES

1. Howell, L.L., *Compliant Mechanisms*, John Wiley & Sons, New York, 2001.
2. Howell, L.L., DiBiasio, C.M., Cullinan, M.A., Panas, R., and Culpepper, M.L., "A pseudo-rigid-body model for large deflections of fixed-clamped carbon nanotubes," *Journal of Mechanisms and Robotics*, Vol. 2, No. 3, pp. 034501, 2010.
3. Hao, G., and Kong, X., "A normalization-based approach to the mobility analysis of spatial compliant multi-beam modules," *Mechanism and Machine Theory*, Vol. 59, pp. 1-19, 2013.
4. Awtar, S., "*Analysis and Synthesis of Planer Kinematic XY Mechanisms*," Sc.D. thesis, Massachusetts Institute of Technology, Cambridge, MA, 2004.
5. Awtar, S., and Slocum, A.H., "Characteristics of beam-based flexure modules", *Journal of Mechanical Design*, Vol. 129, No. 6, pp. 624-639,2007.
6. Zelenika, S. and De Bona, F., "Analytical and experimental characterization of high-precision flexural pivots subjected to lateral loads," *Precision Engineering*, Vol. 26, No. 4, pp. 381-388, 2002.
7. Zhang, A., and Chen, G., "A comprehensive elliptic integral solution to the large deflection problems of thin beams in compliant mechanisms," *Journal of Mechanisms and Robotics*, Vol. 5, No. 2, pp. 021006, 2013.
8. Su, H., "A pseudo-rigid-body 3R model for determining large deflection of cantilever beams subject to tip loads," *Journal of Mechanisms and Robotics*, Vol. 1, No. 2, pp. 021008, 2009.

9. Chen, G., Xiong, B., and Huang, X., "Finding the optimal characteristic parameters for 3R pseudo-rigid-body model using an improved particle swarm optimizer," *Precision Engineering*, Vol. 35, No. 3, pp. 505–511, 2011.
10. Pei, X., Yu, J., Zong, G., and Bi, S., "An effective pseudo-rigid-body method for beam-based compliant mechanisms," *Precision Engineering*, Vol. 34, No. 3, pp. 634-639, 2010.
11. Sen, S., "*Beam Constraint Model: Generalized Nonlinear Closed-form Modeling of Beam Flexures for Flexure Mechanism Design*," Sc.D. thesis, University of Michigan, 2012.
12. Timoshenko, S., and Goodier, J.N., *Theory of Elasticity*, McGraw-Hill, New York, 1951.